Appl. Phys. A (2017) 123:583
DOI 10.1007/s00339-017-1196-7

Applied Physics A
Materials Science & Processing

Polymorphic phase transition and morphotropic phase boundary in $Ba_{1-x}Ca_xTi_{1-y}Zr_yO_3$ ceramics

M. Ben Abdessalem[1] · S. Aydi[1] · A. Aydi[1] · N. Abdelmoula[1] · Z. Sassi[2] · H. Khemakhem[1]

Received: 1 April 2017 / Accepted: 14 August 2017 / Published online: 20 August 2017

Abstract This paper deals with Ca and Zr co-doped $BaTiO_3$ ($BCTZ_{(x,\ y)}$) ($x = 0.1,\ 0.13,\ 0.2$ and $y = 0.05,\ 0.1,\ 0.15$). These ceramics were prepared using the conventional solid state method. The symmetry, dielectric properties, Raman spectroscopy, ferroelectric behavior and piezoelectric effect were examined. X-ray diffraction (XRD) results display that morphotropic boundary occurs from tetragonal to orthorhombic region of $BCZT_{(x=0.1,\ 0.2,\ y=0.05,\ 0.1)}$ and polymorphic phase transitions from tetragonal to orthorhombic, orthorhombic to rhombohedral regions of $BCZT_{(x=0.13,\ y=0.1)}$. The evolution of the Raman spectra was investigated as a function of compositions at room temperature, in correlation with XRD analysis and dielectric measurements. We note that the substitution of Ca in Ba site and Zr ions in Ti site slightly decreased the cubic-tetragonal temperature transition (T_C) and increased the orthorhombic–tetragonal (T_1) and rhombohedral–orthorhombic (T_2) temperatures transitions. The ferroelectric properties were examined by a *P–E* hysteresis loop. The two parameters ΔT_1 and ΔT_2 are defined as $\Delta T_1 = -T_C - T_1$ and $\Delta T_2 = T_C - T_2$, they come close to T_C for $x = 0.13,\ y = 0.1$, which reveals that this composition is around the polymorphic phase. The excellent piezoelectric coefficient of $d_{33} = 288$ pC N^{-1}, the electromechanical coupling factor $k_p = 40\%$, high constant dielectric 9105, coercive field $E_c = 0.32$ (KV mm^{-1}) and remanent polarization $P_r = 0.1$ (μc mm^{-2}) were obtained for composition $x = 0.13, y = 0.1$.

1 Introduction

Pb-based perovskite ferroelectrics, with a general formula ABO_3, such as $Pb(Zr,Ti)O_3$ and $Pb(MgNb)O_3$ have been an industry standard for many decades in electromechanical, electronic and microwave applications [1–3]. Thanks to their high piezoelectric and electromechanical coupling constants, they have attracted the attention of many researchers over the past few years. However, in view of toxicity, the search to find suitable lead-free materials has been launched.

As a typical ferroelectric perovskite, $BaTiO_3$ (BT), has been extensively studied in the electronic industry and used as a passive component in capacitors [4–6]. $BaTiO_3$ perovskite is an important ferroelectric which undergoes the paraelectric–ferroelectric (cubic to tetragonal symmetry) phase transition at 393 K. BT undergoes three consecutive phase transitions from a cubic Pm3m to a tetragonal P4mm at 393 K, then to an orthorhombic Amm2 phase at 278 K, and finally, to rhombohedra R3m phase at 183 K [7, 8].

The high temperature cubic phase is paraelectric, and all low temperature phases are ferroelectric. The reported piezoelectric charge coefficient (d_{33}) of pure $BaTiO_3$ ceramic is 190 pC N^{-1} [9]. On the other hand, this value increases in the vicinity of tetragonal to orthorhombic and orthorhombic to rhombohedral transition temperature, respectively [8].

This piece of information was exploited to achieve high piezoelectric coefficient by tuning the tetragonal to orthorhombic phase transition temperature near room temperature via doping or making solid solution such as

✉ M. Ben Abdessalem
ben.abdessalem.manel@gmail.com

[1] Laboratoire des Matériaux Multifonctionnels et Applications (LaMMA) (LR16ES18), Université de Sfax, Faculté des Sciences de Sfax (FSS), B.P.1171, 3018 Sfax, Tunisia

[2] Laboratoire de Génie Electrique et Ferroélectricité (LGEF) de L'INSA de Lyon, Lyon, France

[10–14]. Gao et al. [15], Tian et al. [16] and Ehmke et al. [17] indicated that the piezoelectric property was enhanced by designing morphotropic phase boundary (MPB) or polymorphic phase transition (PPT) near room temperature. It was noticed that similar results occurred in the $Na_{0.52}K_{0.48}Nb_{0.93}Sb_{0.07}O_3$ [18] and $(K_{0.5}Na_{0.5})_{1-x}$ $LixNbO_3$ [19] systems by bringing the PPT close to room temperature.

Based on the above-mentioned works, the aim of this paper is the elaboration of MPB or PPT in $Ba_{1-x}Ca_{x}$-$Ti_{1-y}Zr_yO_3$ system.

2 Experimental details

The Compounds $Ba_{1-x}Ca_xTi_{1-y}Zr_yO_3$ ($BCZT_{(x,y)}$) ($x = 0.1$, 0.13 and 0.2; $y = 0.05$, 0.1 and 0.15) were prepared by solid state reaction according to the equation (Eq. 1):

$$(1-x)\ BaCO_3 + xCaCO_3 + (1-y)\ TiO_2 + yZrO_2 Ba_{1-x}Ca_xZr_yTi_{1-y}O_3 + CO_2. \quad (1)$$

The different precursors $BaCO_3$, $CaCO_3$, ZrO_2 and TiO_2 (99.0% of purity) were dried at 423 K for 3 h, mixed for 2 h (h) and ground in an agate mortar with a pestle. The calcinations were carried out at 1523 K for 10 h. Subsequently, the obtained powder was mixed for 2 h and pressed into pellets, having 8 mm in diameter and 1 mm in thickness. The final sintering process was conducted at 1693 K for 3 h under air atmosphere.

X-ray powder diffraction was recorded at room temperature in the angular range $10° \leq 2 \leq 80°$ with a 0.01° in 2θ (step and a counting time of 15 s using a Rigaku Ultrax-18 powder diffractometer with Cu Kα radiation ($\lambda_{K\alpha} = 1.54056$ Å).The data were analyzed by the Rietveld method using the "Fullprof" software [20] to assess phase purity and the crystal structures of the material.

The dielectric measurements were performed on ceramic pellets after deposition of gold electrodes on the circular faces by cathodic sputtering. The real part of the dielectric permittivity (ε'_r) of the sample was measured under helium atmosphere as a function of both temperature (150–550 K) and frequency (1–50 kHz) using liquid nitrogen cryostat and an HP4284 impedance automatic analyzer component.

Raman spectra of sintered samples were recorded from 100 to 900 cm^{-1} in a micro-Raman Spectrometer (LABRAM HR-800), working in a backscattering configuration, equipped with an He^+ ion ($\lambda = 633$ nm) laser. The spectral resolution of the system was 3 cm^{-1}. The deconvoluted Raman active modes for BCTZ(x, y) were determined by fitting, using the LabSpec5 software with a combined Lorentzian–Gaussian band shape.

The room temperature ferroelectric polarization was investigated using a TF Analyzer 1000 aixACCT, at 1 Hz and with an applied electric field of 3 kV mm^{-1}, and 5 K as cooling rate. The piezoelectric at room temperature was evaluated on measuring the d_{33} parameter.

3 Results and discussion

3.1 X-ray powder diffraction study

The X-ray diffraction (XRD) patterns of all samples are analyzed and recorded at room temperature and plotted in Fig. 1. All the compositions possess a pure perovskite structure without any secondary phase. The formation of pure perovskite phase suggests that the Ca and Zr have completely diffused into the lattice site of $BaTiO_3$ to form a homogeneous solid solution.

All compositions are considered tetragonal (P4mm), orthorhombic (Pmm2), rhombohedral (R3m) and a Mixture of these three groups for structural refinement. X-ray line profile analysis and available literature on $BaTiO_3$-based materials are the main criteria upon which the choice of space group was decided. The evaluation of the quality of refinement was based on the goodness of the fit indicator χ^2_i, R_p, R_{wp} and R_{exp}. Using the Rietveld refinement method, the obtained results exhibit good agreement between observed XRD patterns and fitted theoretical results (see Fig. 2 as an example). The extended scan of XRD around $2\theta = 44.2°$–$45.8°$ and $2\theta = 65.1°$–$67.0°$ is shown in Figs. 3, 4 and 5. For the three compositions, refinements were first made with a single phase P4mm. The results of refinements are not satisfactory with $\chi^2_i = 4.77$, 5.89 and 3.15 (see Figs. 3a, 4a, 5a). Therefore, we thought to refine with several phases. For both specimens

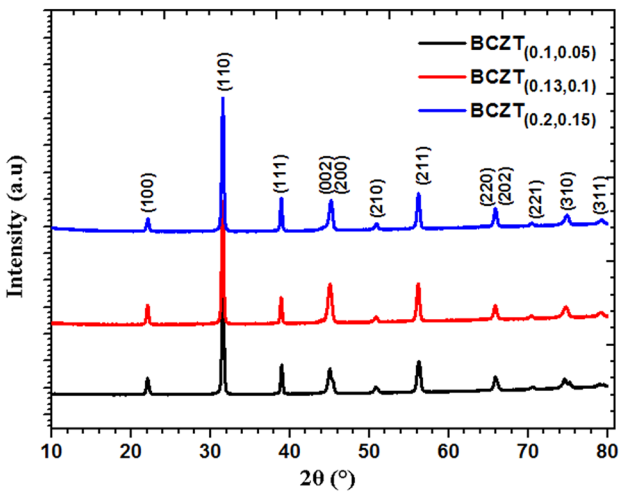

Fig. 1 Powder X-ray diffraction of $BCZT_{(x,\ y)}$ ceramics

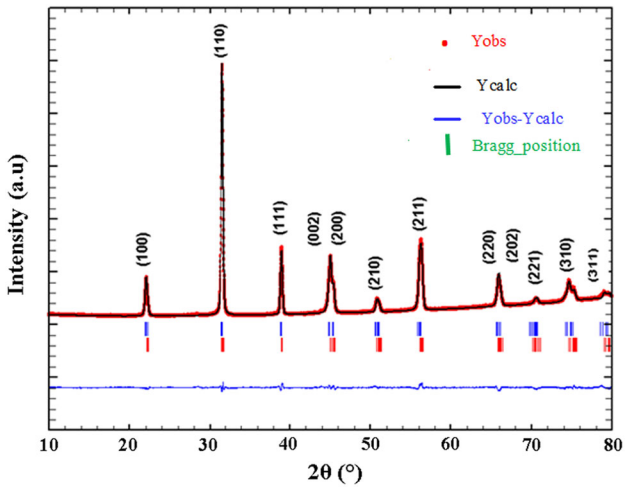

Fig. 2 X-ray diffraction pattern of a $BCZT_{(x,\ y)}$ powder with composition corresponding to $x = 0.1$ and $y = 0.05$

$BCZT_{(0.1,\ 0.05)}$ and $BCZT_{(0.2,\ 0.15)}$, we carried out fit with two-phase models P4mm + Pmm2. The profiles were observed satisfactorily, especially for mixed phases in the peak (200) at 44.4° and 45.8° with $\chi_i^2 = 3.08$ and 0.8 (see Figs. 3b, 5b). The tetragonal fraction is of the order 76.49% for $BCZT_{(0.1,\ 0.05)}$ and 56.41% for $BCZT_{(0.2,\ 0.15)}$. For $BCZT_{(0.13,\ 0.1)}$, we considered a mixture of tetragonal and orthorhombic space groups (P4mm + Pmm2). The fit is not satisfactory in Fig. 4b with $\chi_i^2 = 2.78$. In the next step we considered all three phases tetragonal to orthorhombic to rhombohedra with the space group P4mm + Pmm2 + R3m, simultaneously. This resulted in satisfactory fits of patterns (Fig. 4c) with $\chi_i^2 = 0.9$. From the best fit obtained with the three-phase models, the additional peaks in the peak (200) at 44.4° and 45.8° are clearly characteristic of the P4mm, Pmm2 and R3m phases. The tetragonal fraction is of the order 9.35%.

With reference to Table 1, fitting parameters (R_p, R_{exp}, R_{wp} and χ_i^2) indicate good agreement between refined for all the compositions. The most important difference specimens are in the relative volume fractions of the three coexisting phases. The tetragonal fraction decreased from 76.49 to 9.35%. The Pmm2 fraction increased from 76.92 to 23.51%, respectively. Besides, the substitution of Ca by Ba and Zr by Ti accounts for the structural changes. Indeed, the structural phases switch from tetrahedral system to the orthorhombic one, then to the rhombohedra with an increase of the zirconium and calcium rates. We note that a decrease in the unit cell volume when the composition zirconium and calcium increases. In this case, we can speak about the atomic radii effect in the substitution. Due to fact that the ionic radius of Ca^{2+} (1.34 Å) is smaller than that of Ba^{2+} (1.61 Å) (coordinate with 12 anions) and Zr^{4+} (0.72 Å) is larger than that of Ti^{4+} (0.605 Å) (coordinate with six anions), thus, the substitution of Ba^{2+} by Ca^{2+} and Ti^{4+} with Zr^{4+} could increase the lattice parameter of ceramics [21, 22].

3.2 Raman spectroscopy analysis

Raman spectroscopy is a powerful technique for the study of ferroelectric materials because of the close relationship between ferroelectricity and lattice dynamics [23].

It is an effective method in studying structure effect owing to its sensitivity to local symmetry. To further

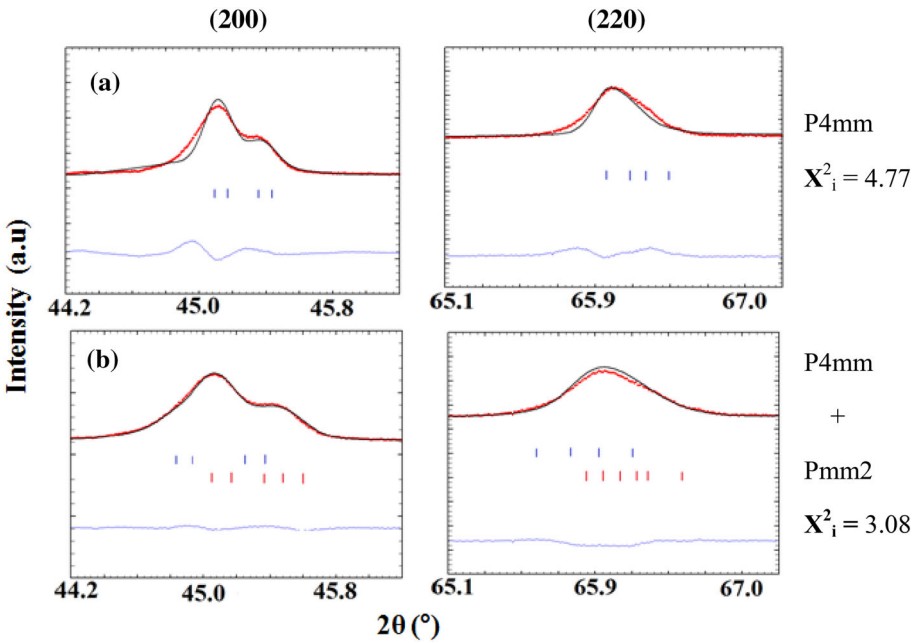

Fig. 3 Rietveld fitted X-ray powder diffraction patterns of $BCZT_{(0.1,\ 0.05)}$ with **a** P4mm and **b** P4mm + Pmm2 models

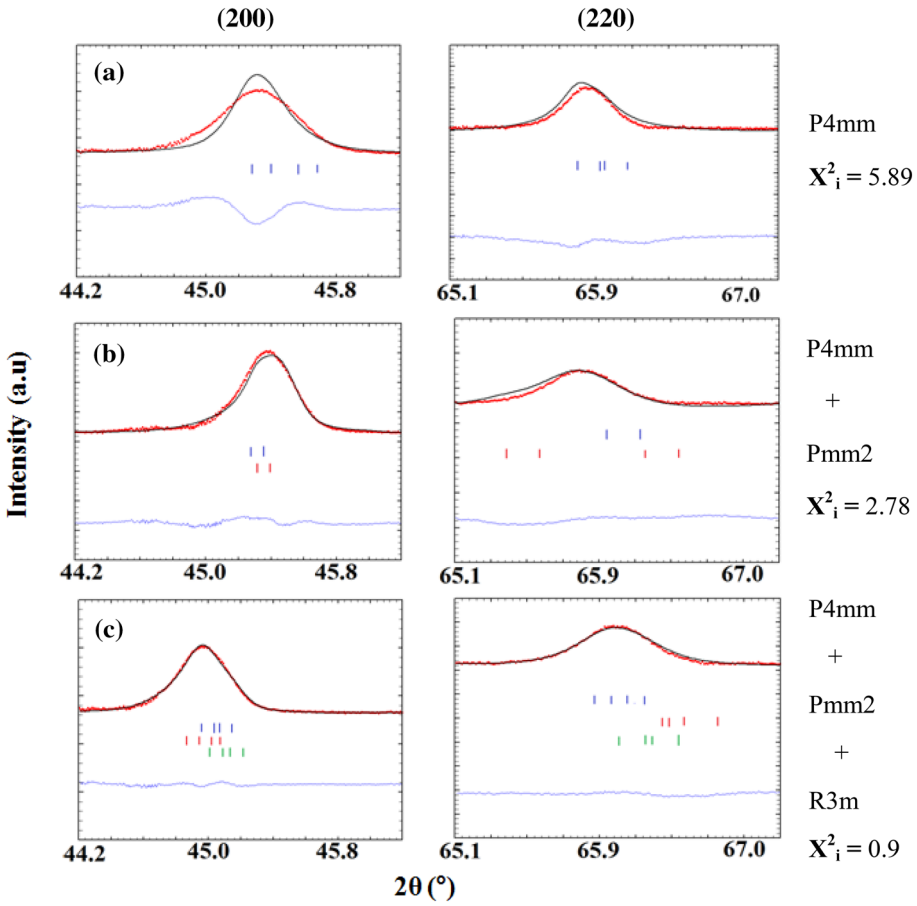

Fig. 4 Rietveld fitted X-ray powder diffraction patterns of $BCZT_{(0.13,\ 0.1)}$ with **a** P4mm, **b** P4mm + Pmm2 and **c** P4mm + Pmm2 + R3m models

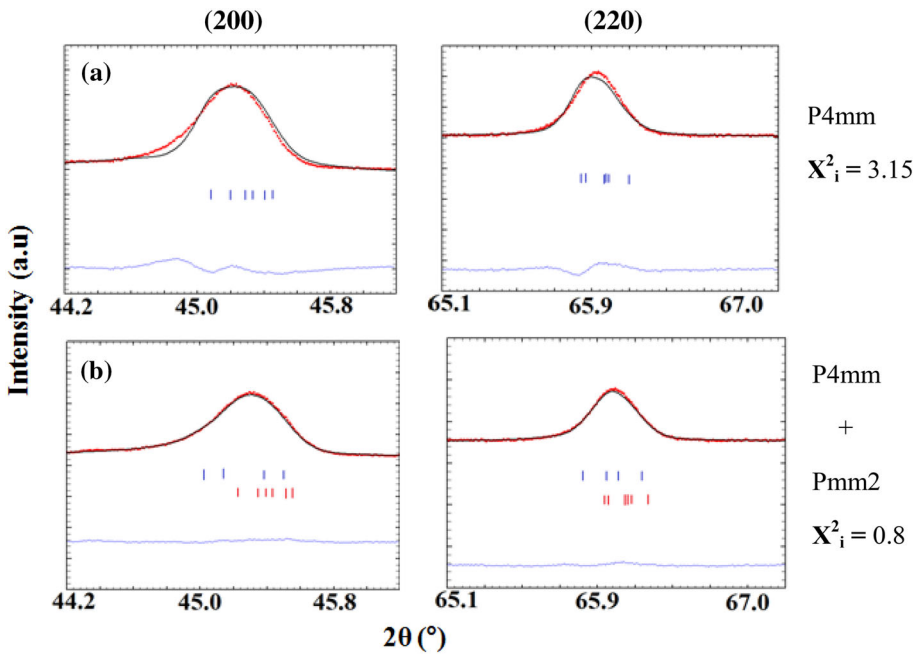

Fig. 5 Rietveld fitted X-ray powder diffraction patterns of $BCZT_{(0.2,\ 0.15)}$ with **a** P4mm and **b** P4mm + Pmm2 models

confirm the phase structure of the $BCZT_{(x,\ y)}$ ceramics, Raman spectroscopy was undertaken, at this stage, to investigate the structure transformation of the specimens. The fitting result Raman spectra of $BCZT_{(x,\ y)}$ with $x = 0.1$ and $y = 0.05$ is shown in Fig. 6 at room temperature.

Table 1 The refined structural parameters for $Ba_{1-x}Ca_xTi_{1-y}Zr_yO_3$

	Space group		
$B_{0.9}Ca_{0.1}Ti_{0.95}Zr_{0.05}O_3$	P4mm	Pmm2	
	$a = b = 4.004(6)$ Å	$a = 3.985(5)$ Å	
	$c = 4.041(5)$ Å	$b = 3.995(1)$ Å	
	$V = 64.8118$ Å^3	$c = 4.021(6)$ Å	
	and % phase = 76.49	$V = 64.0330$ Å^3	
		and % phase = 23.51	
	$R_p = 2.00$, $R_{wp} = 2.65$, $R_{exp} = 1.74$ and $\chi_i^2 = 3.08$		
$B_{0.87}Ca_{0.13}Ti_{0.9}Zr_{0.1}O_3$	P4mm	Pmm2	R3m
	ψ	$a = 4.032(4)$ Å,	$a = b = 5.666(8)$ Å,
	$a = b = 4.028(0)$ Å,	$b = 3.844(1)$ Å,	$c = 6.956(5)$ Å
	$c = 4.02098(1)$ Å	$c = 3.990(0)$ Å	$V = 193.4661$ Å^3
	$V = 64.011(0)$ Å^3	$V = 64.7518$ Å^3	and % phase = 13.73
	and % phase = 9.35	and % phase = 76.92	
	$R_p = 1.73$, $R_{wp} = 2.48$, $R_{exp} = 2.58$ and $\chi_i^2 = 0.9\psi$		
$B_{0.8}Ca_{0.2}Ti_{0.85}Zr_{0.15}O_3$	P4mm	Pmm2	
	$a = b = 4.002(2)$ Å,	$a = 3.997(9)$ Å,	
	$c = 4.032(8)$ Å	$b = 4.001(1)$ Å,	
	$V = 64.594(7)$ Å^3	$c = 4.015(1)$ Å	
	and % phase = 56.41	$V = 64.4796$ Å^3	
		and % phase = 43.59	
	$R_p = 1.28$, $R_{wp} = 1.81$, $R_{exp} = 2.24$ and $\chi_i^2 = 0.8\psi$		

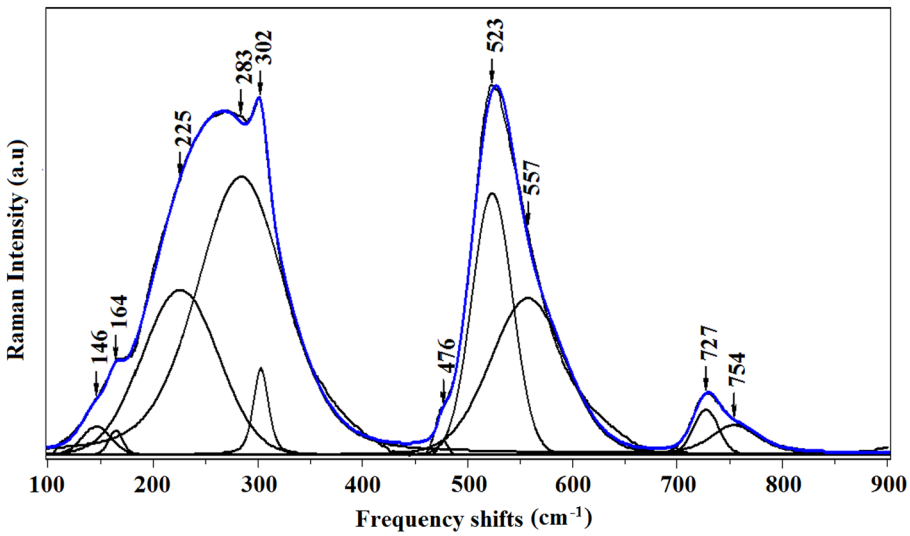

Fig. 6 Raman spectra of the ceramic $BCZT_{(0.1,\ 0.05)}$ at room temperature

$BCZT_{(x,\ y)}$ has a basic matrix of $BaTiO_3$ (BTO) with perovskite structure. Therefore, the Raman mode assignments are considered the same as of pure $BaTiO_3$. The Raman spectra of the BTO is distinguished by dominant bands with positions at 165 cm^{-1} [A_1(TO)], 250 cm^{-1} [A_1(TO)], 307 cm^{-1} [B_1, E (TO + LO)], 470 cm^{-1} [E(TO) + A(LO)], 515 cm^{-1} [A_1(TO), E(TO)], and 715 cm^{-1} [A_1(LO), E(LO)], respectively [24–26].The Raman spectra of the tetragonal BT phase can also contain weak bands at 185 cm^{-1} [A_1 (TO)] and a negative dip at 180 cm^{-1} [E(TO), E(LO)]. The clear peak at 104 cm^{-1} [E(TO_1)], 168 cm^{-1} [$A_1(TO_1)$], 173 cm^{-1} [E(LO_1)], 185 cm^{-1} [$A_1(LO_1)$], and 260 [A_1(TO)]cm^{-1} indicate the rhombohedral (*R*) phase [22, 27, 28]. The 485 cm^{-1} mode loses its intensity around the orthorhombic/tetragonal (*O*/*T*) transition [29]. The intensity of the bands at 307 and 715 cm^{-1} is attributed to the tetragonal/cubic (*T*/*C*) phase transformation [30]. The band at 300 cm^{-1} was assigned to the *B*1 mode, showing asymmetry within the [TiO_6] octahedral, while the band at 725 cm^{-1} was ascribed to the highest wave number of the longitudinal optical mode

(LO) of A_1 symmetry. Although the observation of these two bands clearly confirms the presence of the tetragonal phase, this does not exclude possible phase coexistence [4]. In accordance with these results, the distinctive difference in Table 2 to three samples is noted.

For $BCZT_{(0.1,\ 0.05)}$, the sharp peak at 301 cm^{-1} and the asymmetric broader bands at 523 and 727 cm^{-1}, these bands indicate that they are of tetragonal phase. The peak 476 cm^{-1} is very apparent around the orthorhombic phase. The peak 283 cm^{-1} is considered as a mixture of tetragonal and orthorhombic ($T + O$). In contrast, the peaks at 146 and 163 cm^{-1} are weak which displays a rhombohedral phase.

For $BCTZ_{(0.13,\ 0.1)}$, the weak peak at 299 cm^{-1} and the asymmetric broader bands at 521 and 725 cm^{-1}, these bands are of tetragonal phase. The peak 256 cm^{-1} is apparent around the orthorhombic phase. The peaks 292 and 479 cm^{-1} are clearly revealed during the phase transition from O to T. By contrast, the peak 150, 160 cm^{-1} became very intense broad indication of rhombohedral phase. Carefully examined, the relative intensity of $BCZT_{(0.13,\ 0.1)}$ modes increases while that of $BCZT_{(0.1,\ 0.05)}$ modes decreases. Therefore, rhombohedral phase is well determined in the compound $BCTZ_{(0.13,\ 0.1)}$. For $BCZT_{(0.2,\ 0.15)}$, the sharp peak at 295 cm^{-1} and the asymmetric broader bands at 524 and 726 cm^{-1}, these bands indicate that they are of tetragonal phase. The peak 476 cm^{-1} is very apparent around the orthorhombic phase. The peak 288 cm^{-1} is considered as mixture of tetragonal and orthorhombic ($T + O$). In contrast, the peaks at 146 and 163 cm^{-1} have disappeared. These bands indicate that they are of rhombohedral phase. These results reveal the existence of orthorhombic and tetragonal distortion in the $BCZT_{(0.1,\ 0.05)}$ and $BCZT_{(0.2,\ 0.15)}$ ceramics, which are in good agreement with the XRD patterns.

In $BCZT_{(0.13,\ 0.1)}$, it can be seen that the peak intensity at 262 cm^{-1} is shifted toward lower wave number and it is definitely absent in $BCZT_{(0.1,\ 0.05)}$ and $BCZT_{(0.2,\ 0.15)}$. This behavior is attributed to the rhombohedral to orthorhombic phase transition. The next phase transition, orthorhombic to tetragonal, is carried out at 181 to 194 cm^{-1}. The peak at 190 cm^{-1} is originated from orthorhombic symmetry as observed by the other researchers [32, 33].

The occurrence of the orthorhombic phase at room temperature was previously reported and ascribed to the decrease in grain size [34]. The XRD patterns and Raman spectrum show that the abnormal phenomenon appears for both ceramic with $BCZT_{(0.1,\ 0.05)}$ and $BCZT_{(0.2,\ 0.15)}$, approving that a transition morphotropic phase boundary (MPB) is included in such a ceramic system. Even so, the polymorphic phase transitions (PPT) corresponding tetragonal to orthorhombic and orthorhombic to rhombohedral are seen in $BCTZ_{(0.13,\ 0.1)}$.

The peaks around 523 and 727 cm^{-1} correspond to phonon vibrations of the Ba–O bonds, while the peaks in the range 180–300 cm^{-1} correspond to the phonon vibrations of Ti–O bonds.

A weak Raman active asymmetric breathing mode (A_{1g}) was seen at 803–801 cm^{-1} for $BCZT_{(0.13,\ 0.1)}$ and $BCZT_{(0.2,\ 0.15)}$ while this mode is not prominent for $BCZT_{(0.1,\ 0.05)}$. The broad peak around 803 cm^{-1} was also reported in literature for different $BCZT_{(x,\ y)}$ compositions

Table 2 Obtained optical modes and structure from the Raman at room temperature of $BCZT_{(x,\ y)}$ ceramics

Wave number (cm^{-1})			Assignment	Structure	References
$BCZT_{(0.1,\ 0.05)}$	$BCZT_{(0.13,\ 0.1)}$	$BCZT_{(0.2,\ 0.15)}$			
146	150	–	[$E(TO_1)$]	R	[30, 31]
163	162	–	[$A_1(TO)$]	R	[30, 31]
–	181	–	[$A_1(LO_1)$]	O, T	
–	194	195	[$A_1(LO_1)$]	O	[35]
–	217	–	[$A_1(LO)$, $A_1(TO)$]	O, T	[35]
225	226	–	[$A_1(TO)$]	R	[30, 31]
–	256	244	[$A_1(TO)$]	O	[14, 15, 20, 24]
–	262	–	[$A_1(TO)$]	O, R	[30, 31]
283	292	288	[$E(TO + LO)$]	O, T	[35]
301	299	295	[B_1, $E(TO + LO)$]	T, C	[14, 15, 20, 24]
476	479	476	[$E(TO) + A(LO)$]	O, T	[35]
523	521	524	[$A_1(TO)$, $E(TO)$]	T, C	[14, 15, 20, 24]
561	559	555	[$E(TO4)$]	T, C	[36]
727	725	726	[$A_1(LO)$, $E(LO)$]	T, C	[14, 15, 20, 24]
757	756	752	[$A_1(LO)$, $E(LO)$]	T, C	[35]
_	803	801	A_{1g}	C	[34]

and it is assigned to the presence of several dissimilar atoms at A-sites and B-sites forming a complex perovskite solid solution [35].

Presence of A_{1g} mode in $Ba_{1-x}Ca_xTiO_3$ ceramics might be attributed to the greater amount of Ca^{2+} on the Ba^{2+}site (A) than its solid solubility limit. Additionally, we predict that Ca^{2+} ions partially migrated into both Ba^{2+}, as well as Ti^{4+} sites due to solid solubility limit $x = 0.25$ [36]. Besides, the Raman mode observed at around 292–299 cm^{-1} is shifted to the lower frequency region with the increase in Zr content in $BCZT_{(x,\ y)}$, which can be ascribed to the asymmetric Ti–O phonon vibrations. Improved peaks in $BCZT_{(x,\ y)}$ at a higher frequency compared to BTO, especially 523 and 727 cm^{-1}, is expected due to the difference in ionic radius between Ba^{2+} and Ca^{2+} and Ti^{4+} and Zr^{4+} which leads to the deformation of the lattice and results in enlargement of energy band widening. This shift is also related to the lowering of the Curie temperature. The X-ray diffraction patterns and Raman spectrum show that the unusual phenomenon appears for the $BCZT_{(0.13,\ 0.1)}$ ceramic, confirming the involvement of a phase transition in such ceramic system.

3.3 Dielectric measurement

Figure 7 displays the curves of thermal and frequencies dependences of the dielectric permittivity, wherein all compounds exhibit a classical ferroelectric behavior. As observed, the real part of the dielectric permittivity presents a narrow peak at Curie temperature (T_C) with no frequency dependence.

The dielectric loss decreases with the increase in frequency. To further understand the phase transitions, the differential dielectric permittivity $\left(\frac{\partial \varepsilon_r}{\partial T}\right)$ as a function of temperature is plotted (insets Fig. 7) for three compositions. On the one hand, the decrease in T_C may be attributed to the weakening of the bonding force between the B-site ion and the oxygen ion and the distortion of the octahedron in the ABO_3 type perovskites after the substitution of Zr^{4+} for Ti^{4+}. On the other hand, the addition of Ca^{2+} in A-site has a weak influence on T_C.

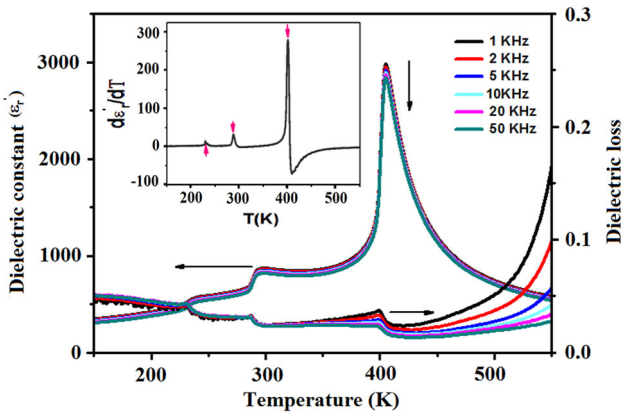

Fig. 7 Temperature dependence of the dielectric permittivity and dielectric loss for $BCZT_{(0.1,\ 0.05)}$ ceramics (*insets* show the differential dielectric permittivity as a function of temperature)

The three anomalies related to the phase transitions (rhombohedral–orthorhombic at T_2, orthorhombic–tetragonal at T_1 and tetragonal–cubic at T_C) for $BaTiO_3$ [37] were observed in three compositions (see Fig. 8). The values of T_1, T_2 and T_C were independent from frequency. The maximum of dielectric permittivity $\varepsilon'_{r\,max}$ increases and the T_C decreases with the augmentation of the zirconium (Zr) and calcium (Ca) content (x, y). Simultaneously, T_1 and T_2 approach to T_C for $BCZT_{(0.13,\ 0.1)}$ and $BCZT_{(0.2,\ 0.15)}$. However, they move away from T_C for $BCZT_{(0.1,\ 0.05)}$. It is noteworthy that these points are very important in morphotropic phase or polymorphic phase. This phase is characterized by the rapprochement of T_1, T_2 and T_c.

In this part, our study focuses on the evolution of T_C, T_1 and T_2 as a function of (x and y). The two parameters ΔT_1 and ΔT_2 are defined as $\Delta T_1 = T_C - T_1$ and $\Delta T_2 = T_C - T_2$ (see Fig. 8). We note that ΔT_1 and ΔT_2 are far away for $BCZT_{(0.1,\ 0.05)}$ and $BCZT_{(0.2;\ 0.15)}$. However, they come close to T_C for $x = 0.13, y = 0.1$. Thus, this composition is around the polymorphic phase. This confirms the XRD analysis. Both the dielectric and X-ray diffraction measurements indicate that the anomaly in dielectric properties is caused by the presence of a PPT near room temperature.

3.4 Ferroelectric and piezoelectric properties

The ferroelectric behavior of our compounds was examined by the measurement of polarization versus electric field (P–E) hysteresis loops at room temperature. The P–

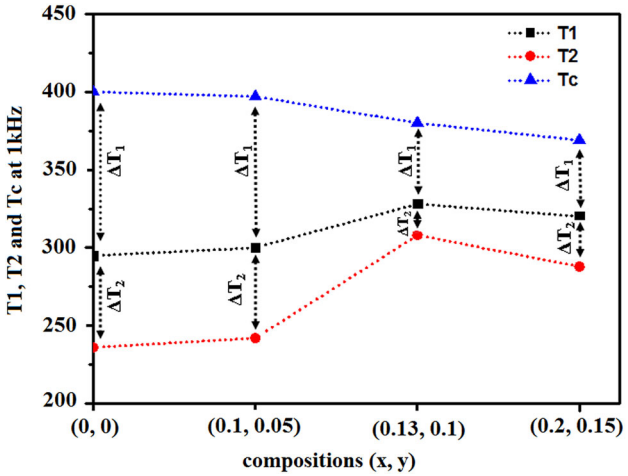

Fig. 8 Plot of T_1, T_2 and T_c as a function of compositions (x, y) at frequency 1 kHz

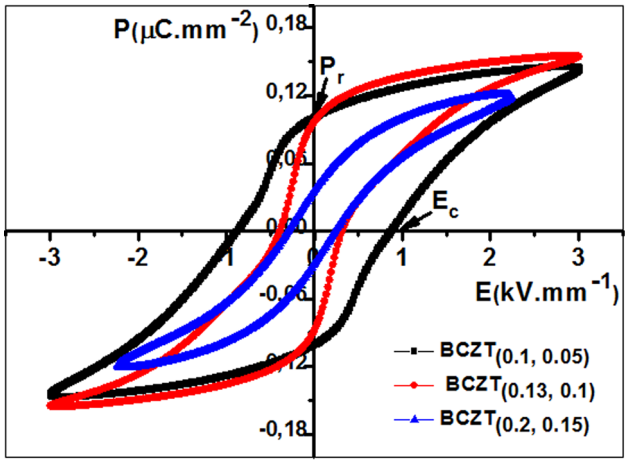

Fig. 9 *P–E* hysteresis loops of $BCZT_{(x,\ y)}$ ceramics with different compositions ($x = 0.1$, 0.13, 0.2 and $y = 0.05$, 0.1, 0.15) at room temperature

E loops measured for $BCZT_{(0.1,\ 0.05)}$ and $BCZT_{(0.13,\ 0.1)}$ under 3 kV mm^{-1} and for $BCZT_{(0.2,\ 0.15)}$ under 2 kV mm^{-1} are reported in Fig. 9. All electrical parameters obtained for $BCZT_{(x,\ y)}$ ceramics are gathered in Table 3.

From hysteresis curves, it is noticed that the remanent polarization (P_r) increases gradually, reaching a maximum value of 0.1 μC mm^{-2} at $x = 0.13$ and $y = 0.1$, and then decreases with further increasing the zirconium and calcium content. This result confirms that the $BCZT_{(0.13,\ 0.1)}$ ceramics with the coexistence of three-phases ($T + O + R$) and two-phase coexisted system ($T + O$) at near room temperature have a higher P_r value than those of the ceramics with other compositions. On the other hand, their coercive field E_c values decrease in accordance with increasing the Zr content. The ceramic with $x = 0.13$ and $y = 0.1$ has a low coercive field of $E_c \sim 0.32$ kV mm^{-1}, showing that the ceramic is "sensitive" to the electric field. These values are better than that given by Abolfazl Jalalian et al. [31].

The piezoelectric coefficient (d_{33}) and planar mode electromechanical coupling coefficient (k_p) values of $BCZT_{(x,\ y)}$ ceramics with different contents were measured at room temperature as illustrated in Table 3. The d_{33} value gradually increases, reaches a maximum at $BCZT_{(0.13,\ 0.1)}$, and drops with increasing zirconium and calcium contents. Similar to the change of d_{33} value, the k_p value also gets a maximum at $BCZT_{(0.13,\ 0.1)}$. Consequently, this ceramic is characterized by an enhanced piezoelectric behavior of $d_{33} = 288$ pC N^{-1} and $k_p = 40\%$, which is ascribed to the complex phases structures of *T*, *O* and *R* near room temperature. It is well known that a two-phase or multiphase boundary can supply a favorable condition for easier motion of domains, thus taking part in the high piezoelectric properties [38]. Moreover, multiphase coexisting sample is characterized by almost an absence of energy barrier for polarization rotation and extension between different ferroelectric phases, which facilitates tremendously the polarization rotation and extension, resulting in high piezoelectric coefficient [39].

The d_{33} value of our $BCZT_{(0.13,\ 0.1)}$ ceramic is much higher than those reported results of $BCZT_{(x,\ y)}$ ceramics. The piezoelectric parameters of $BCZT_{(x,\ y)}$ ceramics are listed in Table 3. The poling field varies from 1 to 3 kV mm^{-1}; the piezoelectric constant (d_{33}) grows with the rising of poling field for $BCZT_{(0.13,\ 0.1)}$. The d_{33} increases with the increase of electrical field from 1 to 2 kV mm^{-1} proving that the poling field is a significant factor, affecting the piezoelectric properties of $BCZT_{(x,\ y)}$ ceramics. For our samples, the optimum field is 3 kV mm^{-1} at room temperature. Besides, the piezoelectric coefficient (d_{33}) decreases and becomes 70 pC N^{-1} for $BCZT_{(0.2,\ 0.15)}$. This can be explained by the stabilization at room temperature of symmetric structure and paraelectric phase.

4 Conclusion

To conclude, $BCZT_{(x,\ y)}$ ceramics with compositions ($x = 0.1$, $y = 0.05$); ($x = 0.13$, $y = 0.10$) and ($x = 0.2$, $y = 0.15$) were prepared using a solid reaction method. The coexistence of tetragonal, orthorhombic and

Table 3 Summary of the various physical properties of $Ba_{1-x}Ca_xTi_{1-y}Zr_yO_3$ ceramics

Sample types	$Ba_{0.9}Ca_{0.1}Zr_{0.05}Ti_{0.95}$	$Ba_{0.87}Ca_{0.13}Zr_{0.1}Ti_{0.9}$	$Ba_{0.8}Ca_{0.2}Zr_{0.15}Ti_{0.85}$
ε'_r at T_c	4865	9105	6201
T_C (K)	393	380	369
P_r (μc mm^{-2})	0.09	0.1	0.04
E_c (kV mm^{-1})	0.87	0.32	0.23
K_p (%)	26	40	14
d_{33}(pC N^{-1}) at 1 kV mm^{-1}	129	231	33
d_{33} (pC N^{-1}) at 2 kV mm^{-1}	184	268	40
d_{33} (pC N^{-1}) at 3 kV mm^{-1}	195	288	70

rhombohedral phases is identified for the $BCZT_{(x,\ y)}$ ceramic at $x = 0.13$ and $y = 0.1$, confirmed by the XRD patterns, the Raman spectroscopy, and the temperature dependence of the dielectric behavior. The fraction of tetragonal phase decreases from 76.49% for $x = 0.1$ and $y = 0.05$–9.35% for $x = 0.13$ and $y = 0.1$. The $BCZT_{(0.13,\ 0.1)}$ ceramics exhibits good piezoelectric properties: $d_{33} = 288$ pC N^{-1}, $k_p = 40\%$, $\varepsilon'_r = 9105$, $E_c = 0.32$ (kV mm^{-1}) and $P_r = 0.09$ (μC mm^{-2}) with a high Curie temperature of 380 K. The enhanced dielectric and piezoelectric coefficients were explained by the coexistence region of the orthorhombic and tetragonal phases owing to the multiplication of the numbers of possible orientations of spontaneous polarization in this region.

References

1. B. Noheda, D.E. Cox, G. Shirane, J. Gao, Z.-G. Ye, Phase diagram of the ferroelectric relaxor (1 − x) $PbMg_{1/3}Nb_{2/3}O_3$–x$PbTiO_3$. Phys. Rev. B **66**, 054104 (2002)
2. N. Setter, D. Damjanovic, L. Eng, G. Fox, S. Gevorgian, S. Hong, A. Kingon, H. Kohlstedt, N.Y. Park, G.B. Stephenson, I. Stolitchnov, A.K. Taganstev, D.V. Taylor, T. Yamada, S. Streiffer, Ferroelectric thin films: review of materials, properties, and applications. J. Appl. Phys. **100**, 051606–051646 (2006)
3. Z. Kutnjak, J. Petzelt, R. Blinc, The giant electromechanical response in ferroelectric relaxors as a critical phenomenon. Nature **441**, 956–959 (2006)
4. H. Zaghouene, H. Khemakhem, A. Simon, X-ray diffraction, dielectric, pyroelectric, piezoelectric and Raman spectroscopy studies on $(Ba_{0.95}Ca_{0.05})_{0.8875}Bi_{0.075}TiO_3$ ceramic. Ceram. Int. **38**, 3135–3139 (2012)
5. L. Zhou, P.M. Vilarinho, J.L. Baptista, Role of defects on the aging behavior of manganese-doped lead iron tungstate relaxor ceramics. J. Am. Ceram. Soc. **83**, 413–414 (2000)
6. S.H. Choy, W.K. Li, H.K. Li, K.H. Lam, H.L.W. Chan, Study of BNKLBT-1.5 lead-free ceramic/epoxy 1-3 composites. J. Appl. Phys. **102**, 1–5 (2007)
7. R. Bechmann, Elastic, piezoelectric, and dielectric constants of polarized barium titanate ceramics and some applications of the piezoelectric equations. Acoust. Soc. Am. **28**, 347–350 (1956)
8. T. Takenaka, H. Nagata, Current status and prospects of lead-free piezoelectric ceramics. J. Eur. Ceram. Soc. **25**, 2693–2700 (2005)
9. T.R. Shrout, S.J. Zhang, Lead-free piezoelectric ceramics: alternatives for PZT? J. Electroceram. **19**, 113–126 (2007)
10. Z. Yu, C. Ang, R. Guo, A.S. Bhalla, Piezoelectric and strain properties of $Ba(Ti_{1-x}\ Zr_x)O_3$ ceramics. J. Appl. Phys. **92**, 1489–1493 (2002)
11. S. Su, R. Zuo, S. Lu, Z. Xu, X. Wang, L. Li, Poling dependence and stability of piezoelectric properties of $Ba(Zr_{0.2}Ti_{0.8})O_3$–$(Ba_{0.7}Ca_{0.3})TiO_3$ ceramics with huge piezoelectric coefficients. Curr. Appl. Phys. **11**, S120–S123 (2011)
12. W. Liu, X. Ren, Large piezoelectric effect in Pb-free ceramics. Phys. Rev. Lett. **103**, 257602–257604 (2009)
13. J. Wu, D. Xiao, W. Wu, Q. Chen, J. Zhu, Z. Yang, J. Wang, Role of room-temperature phase transition in the electrical properties of (Ba, Ca)(Ti, Zr)O_3 ceramics. Scripta Mater. **65**, 771–774 (2011)
14. P. Wang, Y. Li, Y. Lu, Enhanced piezoelectric properties of $(Ba_{0.85}Ca_{0.15})(Ti_{0.9}Zr_{0.1})O_3$ lead-free ceramics by optimizing calcinations and sintering temperature. J. Eur. Ceram. Soc. **31**, 2005–2012 (2011)
15. J. Gao, D. Xue, Y. Wang, D. Wang, L. Zhang, H. Wu, S. Guo, H. Bao, C. Zhou, W. Liu, S. Hou, G. Xiao, X. Ren, Microstructure basis for strong piezoelectricity in Pb-free $Ba(Zr_{0.2}Ti_{0.8})O_3$–$(Ba_{0.7}Ca_{0.3})TiO_3$ ceramics. Appl. Phys. Lett. **99**, 092901 (2011)
16. Y. Tian, L. Wei, X. Chao, Z. Liu, Z. Yang, Phase transition behavior and large piezoelectricity near the morphotropic phase boundary of lead-free $(Ba_{0.85}Ca_{0.15})(Zr_{0.1}Ti_{0.9})O_3$ ceramics. J. Am. Ceram. Soc. **96**(2), 496–502 (2013)
17. M.C. Ehmke, F.H. Schader, K.G. Webber, J. RÖdel, J.E. Blendell, K.J. Bowman, Stress, temperature and electric field effects in the lead-free (Ba, Ca)(Ti, Zr)O_3 piezoelectric system. Acta Mater. **78**, 37–45 (2014)
18. W. Ge, J. Li, D. Viehland, Electric-field-dependent phase volume fractions and enhanced piezoelectricity near the polymorphic phase boundary of $(K_{0.5}Na_{0.5})_{1-x}Li_x$ NbO_3 textured ceramics. Phys. Rev. B **83**, 224110 (2011)
19. F. Jian, R. Zuo, X. Wang, L. Li, Polymorphic phase transition and enhanced piezoelectric properties of $LiTaO_3$ -modified $(Na_{0.52}K_{0.48})$ $(Nb_{0.93}Sb_{0.07})O_3$ lead-free ceramics. J. Phys. D Appl. Phys. **42**, 012006 (2009)
20. A. Simon, J. Ravez, M. Maglione, Relaxor properties of $Ba_{0.9-}Bi_{0.067}(Ti_{1-x}Zr_x)O_3$ ceramics. Solid State Sci. **7**, 925–930 (2005)
21. E. Venkata Ramana, A. Mahajan, M.P.F. Grac, S.K. Mendiratta, J.M. Monteiro, M.A. Valente, Structure and ferroelectric studies of (Ba0.85Ca0.15)(Ti0.9Zr0.1)O_3 piezoelectric ceramics. Mater. Res. Bull. **48**, 4395–4401 (2013)
22. M. Sutapun, W. Vittayakorn, R. Muanghlua, N. Vittayakorn, High piezoelectric response in the new coexistent phase boundary of $0.87BaTiO_3$–(0.13-x)$BaZrO_3$-x$CaTiO_3$. Mater. Des. **86**, 564–574 (2015)
23. M. DiDomenico Jr., S.H. Wemple, S.P.S. Porto, R.P. Bauman, Raman spectrum of single-domain $BaTiO_3$. Phys. Rev. **174**, 522–530 (1968)
24. U.D. Venkateswaran, High-pressure Raman studies of polycrystalline $BaTiO_3$. Phys. Rev. B **58**, 14256–14260 (1998)
25. Y. Shiratori, C. Pithan, J. Dornseiffer, R. Waser, Raman scattering studies on nanocrystalline BaTiO3 Part II-consolidated polycrystalline ceramics. J. Raman Spectrosc. **38**, 1300–1306 (2007)
26. U.M. Pasha, H. Zheng, O.P. Thakur, A. Feteira, K.R. Whittle, D.C. Sinclair, I.M. Reaney, In situ Raman spectroscopy of A-site doped barium titanate. Appl. Phys. Lett. **91**, 062908 (2007)
27. X. Deng, X. Wang, H. Wen, A. Kang, Z. Gui, L. Li, Phase transitions in nanocrystalline barium titanate ceramics prepared by spark plasma sintering. J. Am. Ceram. Soc. **89**, 1059–1064 (2006)
28. P. Ghosez, X. Gonze, J.-P. Michenaud, Coulomb interaction and ferroelectric instability of BaTiO3. Europhys. Lett. **33**, 713–718 (1996)
29. P.S. Dobal, R.S. Katiyar, Studies on ferroelectric perovskites and Bi-layered compounds using micro-Raman spectroscopy. J. Raman Spectrosc. **33**, 405–423 (2002)
30. E. Pytte, Theory of perovskite ferroelectrics. Phys. Rev. B **5**, 3758–3769 (1972)
31. A. Jalalian, A.M. Grishin, X. Wang, S.X. Dou, Fabrication of Ca, Zr doped $BaTiO_3$ ferroelectric nanofibers by electrospinning. Phys. Status Solidi C **9**, 1574–1576 (2012)
32. J. Ghosh, S. Mazumder, Structural phase transitions during high energy ball milling of $BaTiO_3$. Phase Transit. **85**, 694–707 (2012)
33. C.J. Xiao, C.Q. Jin, X.H. Wang, Crystal structure of dense nanocrystalline $BaTiO_3$ ceramics. J. Mater. Chem. Phys. **111**, 209–212 (2008)

34. M.H. Frey, D.A. Payne, Grain-size effect on structure and phase transformations for barium titanate. Phys. Rev. B **54**, 3158–3168 (1996)
35. V.S. Puli, A. Kumar, D.B. Chrisley, M. Tomozawa, J.F. Scott, R.S. Katiyar, Barium zirconate-titanate/barium calcium-titanate ceramics via sol–gel process: novel high-energy-density capacitors. J. Phys. D Appl. Phys. **44**, 395403 (2011)
36. V. Krayzman, I. Levin, J.C. Woicik, F. Bridges, E.J. Nelson, D.C. Sinclair, Ca K-edge X-ray absorption fine structure in $BaTiO_3$–$CaTiO_3$ solid solutions. J. Appl. Phys. **113**, 044106 (2013)
37. L. Khemakhema, A. Kabadou, A. Maalej, A. Ben Salah, A. Simon, M. Maglione, New relaxor ceramic with composition $BaTi_{1-x}(Zn_{1/3}Nb_{2/3})xO_3$. J. Alloy Compd. **452**, 451–455 (2008)
38. J. Hao, W. Bai, W. Li, J. Zhai, Correlation between the microstructure and electrical properties in high-performance $(Ba_{0.85}Ca_{0.15})(Zr_{0.1}Ti_{0.9})O_3$ lead-free piezoelectric ceramics. J. Am. Ceram. Soc. **95**, 1–9 (2012)
39. X. Wang, P. Liang, L. Wei, X. Chao, Z. Yang, Phase evolution and enhanced electrical properties of $Ba_{0.85}Ca_{0.15-x}Y_xZr_{0.1}Ti_{0.9}O_3$ lead-free ceramics. J. Mater. Sci. Mater. Electron. **26**(7), 5217–5225 (2015)